# Incremental response of a model granular material by stress probing with DEM simulations

Francesco Froiio, Jean-Noël Roux

.

# Incremental response of a model granular material by stress probing with DEM simulations

F. Froiio * and J.-N. Roux †

*Ecole Centrale de Lyon Centrale de Lyon, Laboratoire de Tribologie et Dynamique des Systèmes
36, avenue Guy de Collongue
69134 Ecully CEDEX, FRANCE
† Université Paris-Est, Laboratoire Navier
2 Allée Kepler, Cité Descartes
77420 Champs-sur-Marne, FRANCE

**Abstract.** We use DEM simulations on a simple 2D model of a granular material to test for the applicability of the classical concepts of elastoplasticity ( e.g., yield criterion, flow rule) to the response to stress increments of arbitrary directions. We apply stress probes in a three-dimensional stress space to various intermediate states (investigation points) along the biaxial compression path, and pay special attention to the influence of the magnitude of the increments. The elastic part of the material response is systematically identified by building the elastic stiffness matrix of well-equilibrated configurations. The influences of the contact stiffness level and of the dominant strain mechanism, contact deformation (I) or network rearrangement (II), are considered. Stress increments sharing the same principal directions as the stress state in the investigation point comply with a standard (single-mechanism) elastoplastic model with a Mohr-Coulomb criterion and well-defined flow rules and plastic moduli. Stress increments with principal axis rotation entail a response which is satisfactorily modeled by superimposing 3 plastic mechanisms, 2 of them symmetrically corresponding to shear stresses of both signs. The full dependence of strain increments on stress increments is thus parametrized with three flow rules, two of which are essentially symmetric.

**Keywords:** Granular materials, Discret Element Method, quasi-static deformation, incremental response, stress probing, principal stress axes rotation
**PACS:** 81.05.Rm, 83.80.Fg

## INTRODUCTION

Elasto-plastic models are insofar the most widely spread continuum models in the literature and in the engineering practice concerned with granular materials under quasi-static loading conditions [1, 2]. These models have been insofar tested, and their parameter fitted, almost exclusively on the basis of phenomenological observation and one still counts a relatively small number of studies investigating the microscopic origin of the macroscopically observed plastic behaviour by discrete, grain-level simulations [3, 4, 5, 6].

Testing the response of representative elementary volumes (REV's) of a given material to "small" stress or strain increments, superimposed in various directions on an equilibrium state is perhaps the most appropriate procedure in order to assess the applicability of a continuum model. This procedure, known under the name of stress probing, is anyway accompanied by some remarkable practical difficulties among which the most important is that one must dispose of as many "identical" specimens as the stress increment directions to be explored (the stress probes). This is the reason why physical experiments of this kind are rare and assessing applicability of elastoplasticity for granular materials makes no exception: the only experimental work following this approach, to the author's knowledge, is the one by Royis and Doanh in 1998 [7] in which the stress probing procedure is applied on specimens issued from CD (Consolidated Drained) triaxial tests on Hostun sand. Using discrete simulations of granular material instead of physical specimens in the stress probing procedure was first proposed by Bardet [8, 9] in 1989 and offers not just an important work-around to these practical difficulties but also endows the stress probing technique with a remarkable flexibility, as we try to show in this work. A more recent study using the stress probing procedure via DEM simulations was authored by Calvetti and coworkers who focused on the elastoplastic behaviour of 3D specimens (assemblages of spheres), subjected to axisymmetric loading history (triaxial test) and stress probes with the same principal directions

as the triaxial test [4, 10, 11]. Similar tests were run by Alonso-Marroquín and coworkers in 2D on polygonal particles [3, 12]. A substantial agreement can be found, among these authors, on the elastoplastic characters of the response of the tested materials, at small strains and with monotonous loading histories from virgin isotropically consolidated states. Two main features were confirmed in particular: the effectiveness, under the considered test conditions, of plastic models based on a single mechanism of plastic deformation and the "non associated" character of the flow rule.

In this work we present some preliminary results of a study which aims at assessing or clarifying other aspects of the elastoplastic response of granular materials, via a similar numerical implementation of the stress probing procedure. We use 2D specimens (assemblages of circular disks) subjected to a standard biaxial compression and then tested against stress probes in various directions of the stress space. The specificity of this work are the following: (i) the study is parametric in that we widen the range of the model parameters to access a number of significantly different classes of mechanical responses; (ii) we systematically test the dependence of the incremental response on the size of the stress increments; (iii) stress probing is performed in a three-dimensional stress space, i.e., we apply stress increments in the plane spanned by principal axes as well as stress increments inducing rotation of the latter (i.e., increments adding amounts of shear stress on principal planes). One motivation of our study is the modelling of localisation in granular media, where the applicability of such criteria as Rudnicki and Rice's may depend on *subtleties of the incremental constitutive description* [22]. As regards point (iii), in particular, let us remark that localisation appears to be crucially sensitive to the stress increments inducing rotation of principal axes, as is the case when some simple shear is superimposed on a biaxial compression [21].

In the remainder of this section we recall the basic ideas of the constitutive model to be assessed. Eventually, we describe the model material and the biaxial test procedure characterising the loading history of the specimens prior to stress probes. The next two sections present our preliminary results concerning the response to stress increments in the plane of principal stress axes and in a general three-dimensional stress space, respectively. The future steps of this study are outlined in the concluding section.

## Notation

The formulas we will be needing in the following use the standard, compact notation convention of continuum mechanics. For ease of reading we will reserve boldface Greek characters to 2nd-order tensors and boldface Latin characters for Euclidean vectors. Interposed dots between two vectors or two tensors will denote the standard scalar product in the inherent linear spaces. As often is the case when dealing with frictional materials, the sign convention adopted here for the Cauchy stress tensor $\boldsymbol{\sigma}$ and for the infinitesimal strain tensor $\boldsymbol{\varepsilon}$ is such that compressive states are measured by positive values of the diagonal elements of stress and strain matrices.

## Constitutive model

In most common scenarios of interest in civil engineering, granular materials are involved as large masses undergoing quasistatic deformation processes and exhibiting a variety of mechanical behaviours, from solid-like to fluid-like depending on the importance of the rearrangement of the contact network among the various microscopic ingredient of the macroscopic deformation. In this work we focus on the behaviour for small amounts of deformation from a virgin state, i.e., $\|\boldsymbol{\varepsilon}\| \sim 0.005$, where $\boldsymbol{\varepsilon}$ is the infinitesimal strain tensor. We postpone to a further publication the analyses for higher deformation levels. Despite some measurable network rearrangement can appear and even contribute substantially to the macroscopic deformation [13, 15, 16], it is commonly accepted that use of continuum models for solids is appropriate within this deformation threshold, provided the constitutive paradigm can take into account the strong irreversibilities and non-linearities that appear since the inception of deformation.

Classical plasticity models were imported in soil mechanics from metal plasticity and adapted to frictional-cohesive materials [17]. A main contribution to the understanding of frictional-cohesive materials was then given by the authors of a class of models grouped under the name of critical state soil mechanics (e.g., [18, 19]). The Cam-clay model and its ancestor the Granta-gravel model were prototypes of this family.

Only a few basic ingredients of the elastoplastic theories for granular materials need to be recalled here. *In primis* one usually mentions the hypothesis of rate-independence of the constitutive behaviour. The latter expresses the fact that the deformation process does not depend on physical time. The corresponding mathematical statement is that the

strain rate is a homogeneous function of degree 1 of the stress rate, i.e.,

$$\forall \lambda > 0 : \quad \dot{\boldsymbol{\varepsilon}}(\lambda\, \dot{\boldsymbol{\sigma}}) = \lambda\, \dot{\boldsymbol{\varepsilon}}(\dot{\boldsymbol{\sigma}})\,. \tag{1}$$

Ensuring quasi-static conditions implies the use of very low time rates, at which this hypothesis is generally satisfied. In terms of stress increments $\delta\boldsymbol{\sigma}$ and strain increments $\delta\boldsymbol{\varepsilon}$, Eq. 1 authorises to write that

$$\forall \lambda > 0 : \quad \delta\boldsymbol{\varepsilon}(\lambda\, \delta\boldsymbol{\sigma}) = \lambda\, \delta\boldsymbol{\varepsilon}(\delta\boldsymbol{\sigma})\,, \tag{2}$$

provided increments $\delta\boldsymbol{\sigma}$ and $\delta\boldsymbol{\varepsilon}$ are small enough to be considered as infinitesimal. How small is "small" is one of the questions raised in this work and we will make use of Eq. 2 as a smallness criterion to filter out "non infinitesimal" stress and strain increments in our experimental procedure.

A second ingredient of plasticity we are interested in is the so-called *partition hypothesis*. We refer to the assumption that the strain increments $\delta\boldsymbol{\varepsilon}$ can be decomposed additively into elastic strain increments $\delta\boldsymbol{\varepsilon}^E$ and plastic strain increments $\delta\boldsymbol{\varepsilon}^P$:

$$\delta\boldsymbol{\varepsilon} = \delta\boldsymbol{\varepsilon}^E + \delta\boldsymbol{\varepsilon}^P \tag{3}$$

The former are computed according to a properly defined elastic compliance tensor $\mathbb{C}$, i.e.,

$$\delta\boldsymbol{\varepsilon}^E = \mathbb{C}\,\delta\boldsymbol{\sigma} \tag{4}$$

and relate to the amount of deformation work $\boldsymbol{\sigma}\cdot\delta\boldsymbol{\varepsilon}$ that is being reversibly stored as elastic energy. The latter relates to the amount of deformation work that is being dissipated and should fit the plastic constitutive assumption as specified here below in terms of a *yield criterion* and a *plastic flow rule*.

The yield criterion gives the recipe to compute plastic strain increments and distinguishes between "active" and "inactive" stress increments with respect to the mechanism responsible for plastic strains. With some simplification in the terminology we refer here to the yield criterion as prescription

$$\|\delta\boldsymbol{\varepsilon}^P\| = \begin{cases} \frac{1}{E^P}\,\delta\boldsymbol{\sigma}\cdot\boldsymbol{\xi} & \text{if} \quad f(\boldsymbol{\sigma}) = 0 \quad \text{and} \quad \delta\boldsymbol{\sigma}\cdot\boldsymbol{\xi} \geq 0 \\ 0 & \text{if} \quad f(\boldsymbol{\sigma}) = 0 \quad \text{and} \quad \delta\boldsymbol{\sigma}\cdot\boldsymbol{\xi} < 0 \\ 0 & \text{if} \quad f(\boldsymbol{\sigma}) < 0 \end{cases} \tag{5}$$

in which the yield locus $f(\boldsymbol{\sigma}) = 0$ has outward oriented unit normal $\boldsymbol{\xi} := \frac{\partial f}{\partial \boldsymbol{\sigma}} \| \frac{\partial f}{\partial \boldsymbol{\sigma}} \|^{-1}$ and bounds the elastic domain in stress space. According to the above criterion, the only stress increments that succeed in producing plastic strain increments are those applied when the current stress state $\boldsymbol{\sigma}$ has reached the yield locus, and that point outward from the elastic domain. If these two conditions are met, the corresponding plastic strain increment will be proportional to the active part of the stress increment, i.e. the component $\delta\boldsymbol{\sigma}\cdot\boldsymbol{\xi}$, through the constant $E^P$ called plastic modulus.

Finally, and once more loosely speaking, the plastic flow rule assigns a unique direction in stress space for all plastic strain increments, i.e., independently on the stress increment direction:

$$\forall \delta\boldsymbol{\sigma} : \quad \delta\,\boldsymbol{\varepsilon}^P(\delta\boldsymbol{\sigma}) = \boldsymbol{\pi}(\boldsymbol{\sigma})\,\|\delta\boldsymbol{\varepsilon}^P(\delta\boldsymbol{\sigma})\| \tag{6}$$

where the tensor $\boldsymbol{\pi}$, $\|\boldsymbol{\pi}\| = 1$, is called *plastic flow direction*.

The particular yield criterion discussed in this work is of the Mohr-Coulomb type: we define function $f$ in Eq. 5 with the expression

$$f = |\mathbf{m}\cdot\boldsymbol{\sigma}\mathbf{n}| - \mu_s\,\mathbf{n}\cdot\boldsymbol{\sigma}\mathbf{n}\,, \quad \mathbf{n}\cdot\mathbf{m} = 0 \tag{7}$$

whose terms can be described by rephrasing a few elements of Batdorf and Budiansky's plastic slip theory for polycrystalline materials [20] in the case of materials with particulate, frictional microstructure. Plastic strains are the macroscopic effect of slips along families of micro-planes inside the specimen (slip planes), characterised in Eq. 5 by an in-plane vector $\mathbf{m}$ (the slip direction) and by the unit normal $\mathbf{n}$. Plastic slip is activated when the threshold of tangential stress is reached on the inherent slip plane. At the scale of the REV this mechanism is reflected by a yield criterion $f = 0$ depending on a friction parameter $\mu_s$. The latter is not a material constant but a parameter that evolves so to ensure $\delta f = 0$ during plastic loading (cf. Eq. 5). Implicit assumptions in Eq. 7 are that $\mathbf{n}\cdot\boldsymbol{\sigma}\mathbf{n} \geq 0$, as customary for non-cohesive granular materials, and that all activated slip planes hold nearly the same orientation.

We remark that some algebra leads to

$$\boldsymbol{\xi} = \pm\frac{1}{2}(\mathbf{m}\otimes\mathbf{n} + \mathbf{n}\otimes\mathbf{m}) - \mu_s\,\mathbf{n}\otimes\mathbf{n} \tag{8}$$

where the sign of the first term on the r.h.s. depends on the way the modulus operator has been resolved in Eq. 7. Using Eq. 8 with this caution we obtain, finally, a more compact form for the first equality in Eq. 7, i.e.,

$$f = \boldsymbol{\xi} \cdot \boldsymbol{\sigma} . \tag{9}$$

## SPECIMEN PREPARATION

We characterise here the different types of specimens whose response under stress probes will be discussed in the following sections. The specimens are grouped into classes, based on non-dimensional control parameters, reflecting both the qualitative type of deformation response and the loading history.

### Model material

The samples in use in our simulations consist of 5600 disks with diameters distributed uniformly between $0.7d$ and $1.3d$, where $d$ is the average, representative diameter. All disks are assumed to be made of a homogeneous material, and $m$ denotes the mass of particles of diameter $d$. The disks are initially arranged in rectangular cells whose wedges align along direction 1 and direction 2: the first is the "confinement" or "lateral" direction and the latter is the "axial" or "vertical" direction, in referring to the usual laboratory conditions of biaxial/triaxial testing. The cell can deform into an arbitrary parallelogram in order to accommodate the generic configuration of a two-dimensional cell undergoing homogeneous deformations at small-strains. Bi-periodicity is obtained, numerically, by an adaptation to DEM simulations of Parrinello-Rahman and Lees-Edwards techniques for molecular dynamics simulations (cf. [23, 24]). By these techniques we implement either mixed boundary conditions (for axial compression during biaxial tests, performed at constant axial strain rate and constant lateral pressure) or simple stress-rate-controlled boundary conditions (for isotropic compression during biaxial tests and for the application of stress probes). Samples are regarded in our analyses as REV's and are characterised macroscopically by the components of the stress tensor $\boldsymbol{\sigma}$ and of the infinitesimal strain tensor $\boldsymbol{\varepsilon}$. The former are computed according to the classical Love formula while the latter are retrieved, as usual, as linearised strain measures for the cell.

We use a standard linearly-elastic Coulomb-friction contact model: the normal contact force writes $F_N = K_N h_N$ where $K_N$ is the normal contact stiffness and $h_N \geq 0$ is the (numerical) interpenetration of contacting disks; $F_T = K_T h_T$ relates the tangential contact force $F_T$ to the relative tangential displacement $h_T$ at contact (computed incrementally) through the tangential contact stiffness $K_T$; finally $|F_T|$ is bounded above by $\mu F_N$ where $\mu$ is the contact friction coefficient. Here we choose $K_T = K_N$ and $\mu = 0.3$. An additional viscous force $F_N^{\alpha} = \alpha_N \dot{h}_N$ adds to the elastic force $F_N$ as customary in DEM simulations, merely as a convenient means to accelerate the approach to equilibrium configurations. To this purpose we set $\alpha_N = 0.9\sqrt{2K_N m}$, where $\sqrt{2K_N m}$ is the critical value for a two-particle system with masses $m$ interacting *via* a spring of stiffness $K_N$. Our focus being on constitutive information, gravity or other non-inertial volume actions are not considered here.

### Loading history

The specimens to which stress probes are applied were first subjected to a standard procedure of strain-rate-controlled biaxial compression up to the desired stress ratio $\varsigma = Q/P$, where $Q$ is the final value of the axial pressure $\sigma_{22}$ and $P$ is the value of confining pressure to which the lateral pressure $\sigma_{11}$ is set during axial loading. Prior to axial loading the specimen were consolidated under isotropic stress conditions up to pressure $P$, starting from loose, randomly agitated "granular gas" configurations.

According to the loading history given above and to the previous characterisation of the model material, dimensional analysis leads to the identification of five independent dimensionless parameters that characterise separate classes of "equivalent" specimens: (i) stiffness parameter $\kappa = K_N/P$ setting the scale of contact deflections, as $h/d \propto \kappa^{-1}$; (ii) stress ratio $\varsigma = Q/P$, as an indicator of the deviatoric stress; (iii) friction coefficient $\mu$; (iv) the damping parameter $\zeta = \alpha_N/\sqrt{2K_N m}$ and (v) inertia parameter $\gamma = \dot{\varepsilon}_{22}\sqrt{m/P}$; (vi) tangential to normal stiffness ratio $K_T/K_N$. We use $\zeta = 0.9$, as anticipated previously, and set $\gamma = 10^{-4}$ in order to approach quasistatic conditions with sufficient accuracy.

**TABLE 1.** Biaxial test families and values of variable parameters.

| Biaxial tests | $\mu_{iso}$ | $\kappa$ | $\varsigma$ (*ca.*) |
|---|---|---|---|
| A3 | 0 | $10^3$ | $1.2, 1.4, 1.6, 1.8$ |
| A4 | | $10^4$ | $1.2, 1.4, 1.6, 1.8$ |
| A5 | | $10^5$ | $1.8, 1.9$ |
| B3 | 0.3 | $10^3$ | $1.2, 1.4, 1.6, 1.8$ |
| B4 | | $10^4$ | $1.2, 1.4, 1.6, 1.8$ |
| B5 | | $10^5$ | $1.2, 1.4, 1.6, 1.8$ |

The friction coefficient is also fixed, i.e. $\mu = 0.3$, as well as ratio $K_T/K_N = 1$, but we let $\kappa$ and $\varsigma$ vary as detailed further on.

To further widen the spectrum of specimen classes we play with the value of contact friction coefficient $\mu_{iso}$ adopted during isotropic consolidation [15]. The only possible choice in real laboratory experiences is of course $\mu_{iso} = \mu$ but the numerical model allows us to set $\mu$ and $\mu_{iso} < \mu$ independently from each other. This possibility (supplemented with an "agitation" stage [15]) can be used as a robust procedure to obtain specimens that are "macroscopically indistinguishable", i.e. share the same solid fraction $\Phi$, but differ markedly in terms of microstructures and deformation responses [13, 14, 16]. "Lubricated conditions" during isotropic consolidations (i.e., $\mu_{iso} = 0$) drive the material towards high values of the coordination number $z$; testing the material in this state gives a characteristic deformation response at small strains where the leading microscopic mechanism is the deformation at contacts (deformation response of type I). Conversely, "non-lubricated conditions" (i.e., $\mu_{iso} = \mu$), with some vibration, will result into much lower coordination numbers and lead to a deformation response dominated by a continuous network rearrangement due to microscopic instabilities (deformation response of type II). The biaxial compression tests considered in this work were all performed with friction coefficient $\mu = 0.3$, irrespective of the value $\mu_{iso}$ employed in sample preparation (i.e., during isotropic compression).

The parameters used in this work are reported in Table 1. The label A3 on the first line refers to a family of ten "equivalent" biaxial tests characterised by $\mu_{iso} = 0$ and $\kappa = 10^3$. They are equivalent in the sense that their preparation procedures differ just by the initial random velocity field at start up of the isotropic consolidation. The values of stress ratio $\varsigma = 1,2$, 1.4, 1.6, 1.8 at the end of the same line refer to the configurations selected during axial loading, designated as specimens for the stress probing procedure. The following lines in the same table report the same information but relative to other choices of parameters $\kappa$ and $\mu_{iso}$. Fig. 1 illustrates the deformation response during axial loading for biaxial tests of families A3, A4 and A5 (type I deformation response) while Fig. 2 gives the same plots for biaxial tests of families B3, B4 and B5 (type II deformation response). A comparison between the two figures allows to visualise the macroscopic effect of the two microscopic deformation mechanisms mentioned above. The small-strain range of curves in Fig. 1 is sensitive to the stiffness parameter $\kappa$: as shown in [16], strains are actually inversely proportional to $\kappa$, for a given stress ratio $\varsigma$. For the cases in Fig. 2, on the other hand, one notices that the macroscopics behaviour, already at small strains, results from microscopic instabilities and does not depend on the stiffness parameter $\kappa$.

## BIAXIAL STRESS PROBES

For each test family in the Table 1, at least two of the ten equivalent biaxial tests have been considered insofar for the anlysis of the incremental response: the respective specimens were tested *via* stress probing in the above range of stress ratios. We present our results discussing case A4 ($\kappa = 10^4$, type I deformation regime, $\varsigma \simeq 1.2$, 1.4, 1.6, 1.8 ) claiming that the qualitative features that we observed were found repeatable in all the other cases, despite the change in control parameters. The section reports on stress probes applied in the plane of principal stress axes, which correspond in our case to a combination of increments of lateral stress $\sigma_{11}$ and of axial stress $\sigma_{22}$. It will be convenient to refer to the representations in the planes $\sigma_{11}$ *vs.* $\sigma_{22}$ or $\varepsilon_{11}$ *vs.* $\varepsilon_{22}$ as to representations in the *biaxial stress plane* or in the *biaxial strain plane*, respectively.

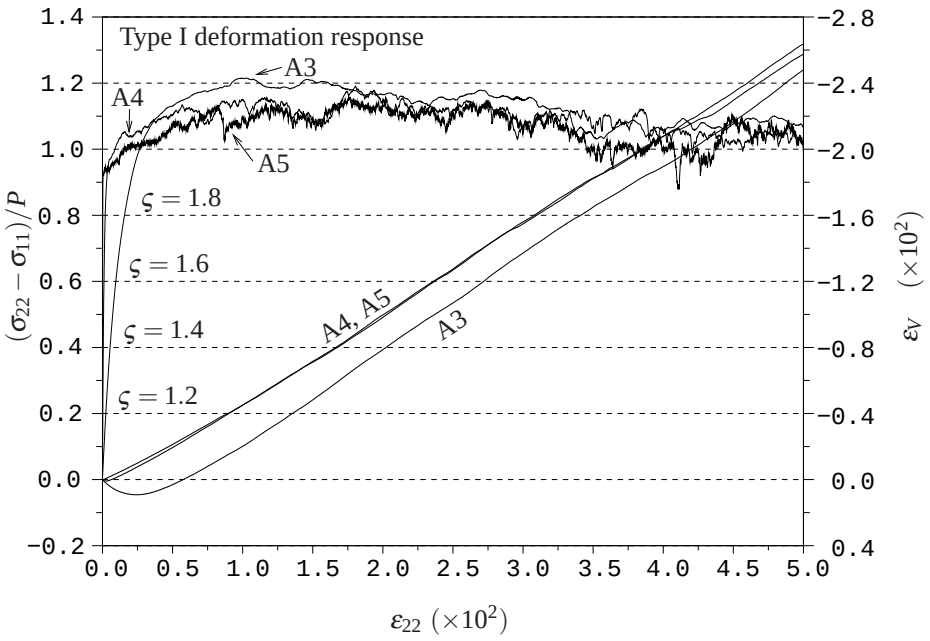


**FIGURE 1.** Normalised deviatoric stress *vs.* axial strain and volumetric strain *vs.* axial strain for typical biaxial tests of families A3, A4 and A5: $\mu_{iso} = 0$ (but $\mu = 0.3$) and $\kappa = 10^3$, $10^4$ and $10^5$, respectively.

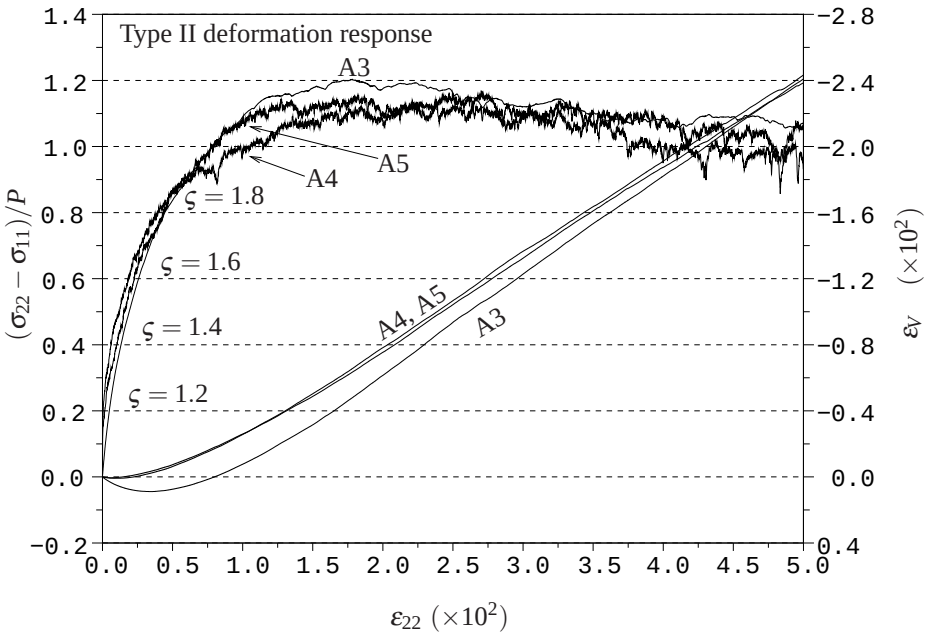


**FIGURE 2.** Normalised deviatoric stress *vs.* axial strain and volumetric strain *vs.* axial strain for typical biaxial tests of families B3, B4 and B5: $\mu_{iso} = \mu = 0.3$ and $\kappa = 10^3$, $10^4$ and $10^5$, respectively.

## Incremental response

The rose of stress increments applied to the specimens is shown in Fig. 3: it consists in twelve increment levels linearly distributed from $\|\delta\boldsymbol{\sigma}\| = 2\sqrt{2}P \times 10^{-3}$ to $12 \times 2\sqrt{2}P \times 10^{-3}$ along sixteen orientations in the biaxial stress plane, labelled from 0A to 0P, with constant angular spacing $2\pi/16$. The elastic response to the increments in Fig. 3

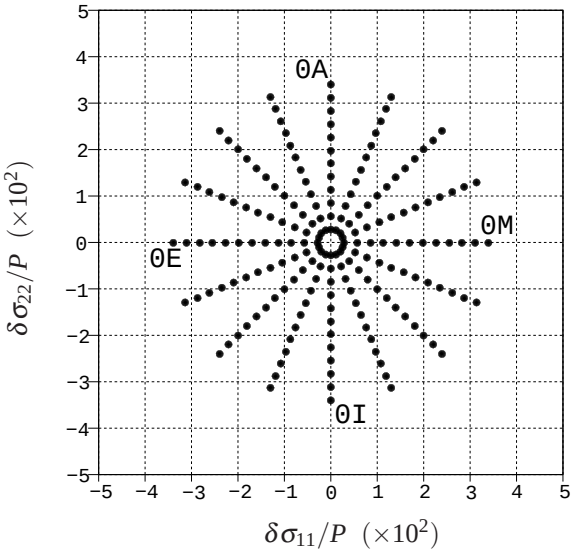


**FIGURE 3.** Rose of applied increments for biaxial stress probing: 16 increment directions (0A to 0P) for 12 amplitude values in the biaxial plane.

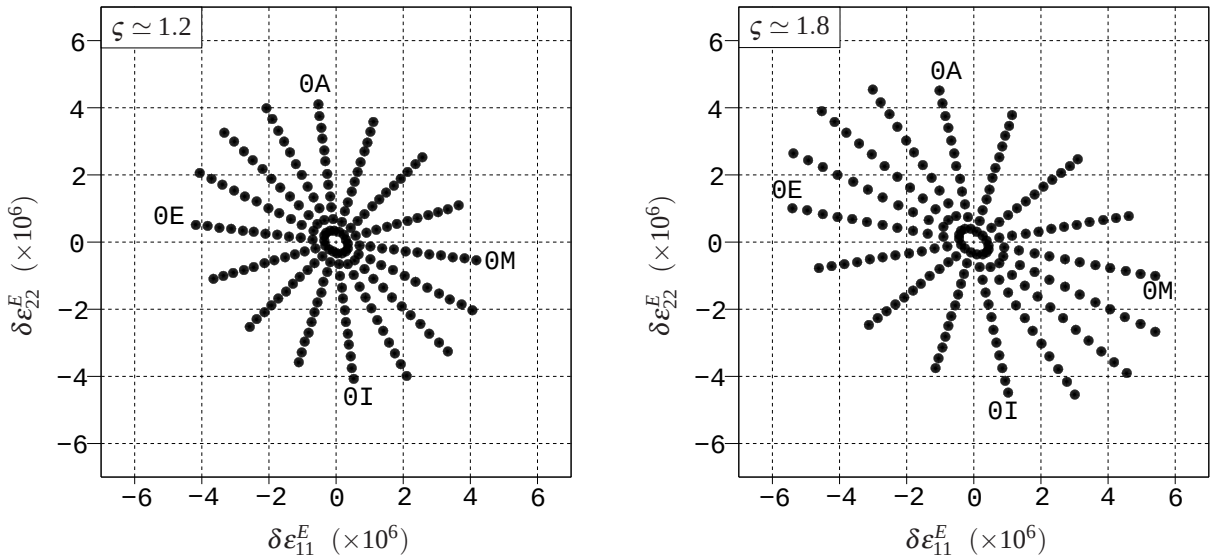


**FIGURE 4.** Elastic response for specimens at stress ratio $\varsigma \simeq 1.2$ (left) and $\varsigma \simeq 1.8$ (right) from a biaxial test of family A4.

is plotted in Fig. 4 for the specimen with lowest and highest values of stress ratio: the material exhibits a marked elastic anisotropy slightly evolving during the axial loading (i.e., from $\varsigma \simeq 1.2$ to 1.8). The elastic strain increments are assumed to be given by the expression in Eq. 4, where the components of the elasticity tensor $\mathbb{C}$ are computed, by assembling the contribution of the contact stiffness $K_N$ and $K_T$ across the contact network [14]. To test the partition hypothesis we identify plastic strain increments to the difference

$$\delta\boldsymbol{\varepsilon}^P = \delta\boldsymbol{\varepsilon} - \delta\boldsymbol{\varepsilon}^E \tag{10}$$

and check *a posteriori* whether or not this definition is effective in giving evidence of a plastic flow rule (cf. Eq 6) and yield criterion (cf. Eq 5).

Fig. 5 shows that the strain increments $\delta\boldsymbol{\varepsilon}^P$ neatly align along a direction in the biaxial strain plane, confirming the applicability of a flow rule. We measure in particular counterclockwise angles of the plastic strain increment direction

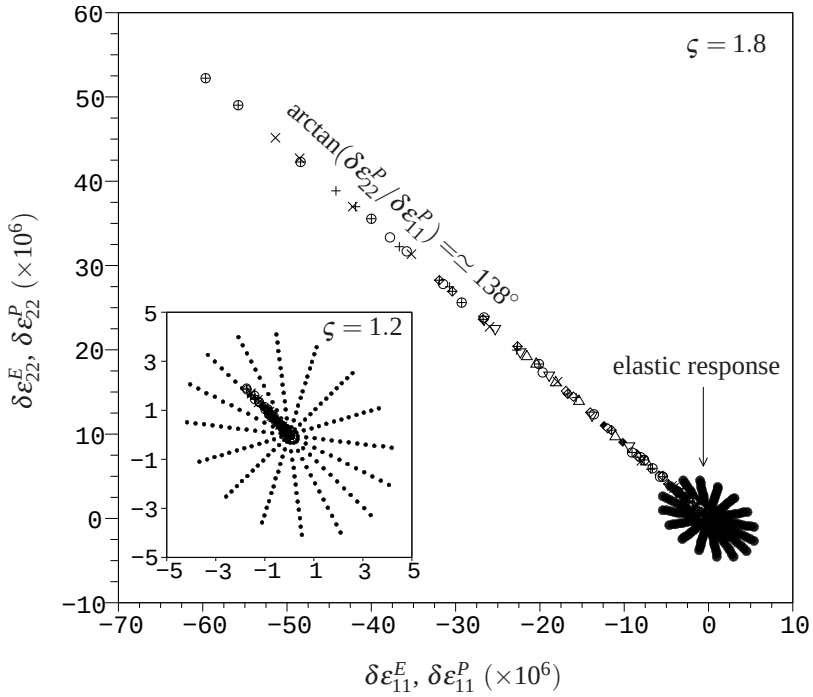


**FIGURE 5.** Elastic vs. plastic response for specimens at stress ratio $\varsigma = 1.2$ (inner window) and $\varsigma = 1.8$ (resp. outer) from a biaxial test of family A4.

with respect to direction $\varepsilon_{11}$, ranging from 132.2° to 138.3° (for $\varsigma \simeq 1.2$ and 1.8, resp.).

To investigate the existence of a yield criterion we consider the case $\varsigma \simeq 1.2$ and plot in Fig. 6 the norm $\|\delta\boldsymbol{\varepsilon}^P\|$ of the plastic strain increment against the angle of the stress increments in the biaxial stress plane. As for the plastic strain increments, stress increment angles in the biaxial plane are measured counterclockwise, with respect to direction "11". The experimental points in Fig. 6 are fitted with a truncated cosine function, expressive of the criterion in Eq 5. The corresponding phase angle (132.3° in the figure) gives the direction of the normal $\boldsymbol{\xi}$ to the supposed yield criterion in the biaxial stress space. The *load direction*, i.e., the direction associated to the current value of the stress tensor $\boldsymbol{\sigma}$ is almost orthogonal to $\boldsymbol{\xi}$, as expected (cf. Eq 9). On the other hand the plastic flow direction $\boldsymbol{\pi}$ is close but not at all coincident with the normal $\boldsymbol{\xi}$ to the yield criterion (separated of about 10°), giving evidence of the non associated character of the flow rule. These two qualitative features were systematically found in all investigated cases: for $\varsigma \simeq 1.2, 1.4, 1.6$ and 1.8, as shown it upper-right quadrant of the same figure, and over the whole range of stress increments. The angles for the direction of the normal $\boldsymbol{\xi}$ to the yield criterion and for the flow direction $\pi$ are compared to the load direction in Table 2.

## Stress increment size

An important question in the stress probing procedure concerns the appropriate size of the strain increments to apply in order to get measurements that are at the same time little affected by systematic errors and representative of the infinitesimal behaviour. To discuss this point we represent in Fig. 7 the norm $\|\delta\boldsymbol{\varepsilon}^P\|$ of the plastic strain increments versus the "active" component of the stress increment, i.e., the positive values of the scalar product $\delta\boldsymbol{\sigma}\cdot\boldsymbol{\xi}$. Fitting the yield criterion in Eq. 5 requires selecting an observation window in which the relation between the norm $\|\delta\boldsymbol{\varepsilon}^P\|$ of the plastic strain increment and the active component of the stress increment can be fitted as linear. The plot in Fig. 7 suggests that, for specimens obtained from biaxial tests of type A4, the size should not exceed the eight-level of

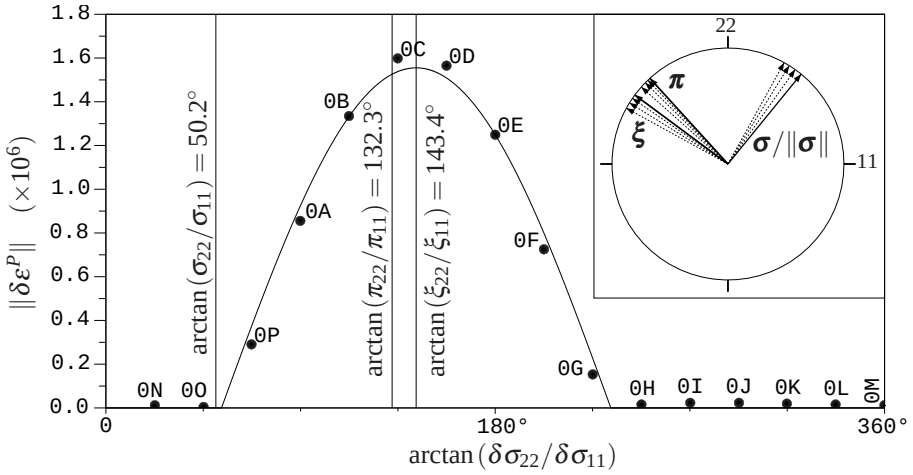


**FIGURE 6.** Fitting of the plastic strain increment amplitude with the truncated cosine function for specimen at stress ratio $\varsigma \simeq 1.2$ (main window) from a biaxial test of family A4. Load direction $\boldsymbol{\sigma}/\|\boldsymbol{\sigma}\|$, normal to the yield criterion $\boldsymbol{\xi}$ and plastic flow direction $\boldsymbol{\pi}$ as they evolve counterclockwise from stress ratio $\varsigma \simeq 1.2$, to 1.8 during the axial loading for the same biaxial test (upper-right window).

increment considered here (i.e., $\|\delta\boldsymbol{\sigma}\| = 8 \times 2\sqrt{2}P \times 10^{-3} \simeq 2.263P \times 10^{-2}$). According to the result analysed insofar by the authors, this range seems also to depend sensitively on the stiffness parameter $\kappa$: the higher the value of the stiffness parameter, the smaller the maximal allowed norm $\|\delta\boldsymbol{\sigma}\|/P$ of the stress increment amplitude. On the other hand it is not advisable to reduce as much as numerically possible the size of the increments, as the case $\varsigma \simeq 1.8$ in the same figure shows: evidence of a residual elastic response is given by the absence of plastic deformation increments in response to very small stress increments. This source of systematic errors can be corrected easily provided "large enough" stress increments are used. Most important this type of systematic error can be explained, mechanically, on the basis of the procedure to which the specimen were subjected prior to to stress probing. We remark in particular that, after the expected value of stress ratio $\varsigma$ is attained during the axial compression, the specimen is left under constant axial and lateral stresses for the time necessary to reach statical equilibrium, not to distort the incremental response during stress probing. A small parasite effect of this intermediate "creep" transition before stress probing is that part of the plastic memory, stored at contact between particles, is erased due to a slight unavoidable rearrangement of the contact network. We expect this effect to gradually fade out as slower and slower numerical tests are performed, in order to approach closer to the quasistatic limit of $\gamma \to 0$. The appreciable non-zero intercept of the (dashed) interpolation line for case $\varsigma \simeq 1.8$ in Fig. 7 can be seen as the macroscopic signature of this mechanism. In the end, an appropriate choice of the size of the increment for stress probing seems to bounded both above, by a linearity requirement, and below, due to a parasite effect of residual elastic behaviour.

## ROTATION OF PRINCIPAL STRESS AXES

The same set of specimens considered in the previous section was tested under stress probes inducing rotation of principal stress axes. We discuss here a few preliminary results, and possible interpretations, that we expect to study systematically on a larger base. The stress space to which we refer is now the general stress space with coordinates $\sigma_{11}$, $\sigma_{22}$ and $\sigma_{12}$, where $\sigma_{12}$ is the third component of the stress tensor, dismissed insofar and corresponding to tangential stresses along the planes orthogonal to the lateral and axial direction. Analogously, the deformation response is measured in a three-dimensional strain space with coordinates $\varepsilon_{11}$, $\varepsilon_{22}$ and $\varepsilon_{12}$.

### Plastic flow direction

For this preliminary analysis, the stress increments lay in a specific plane of the stress space: the plane spanned by the direction of the normal to the yield criterion $\boldsymbol{\xi}$, detected previously, and by the direction associated to the

**TABLE 2.** Load direction, normal to yield criterion and flow direction for tested specimens from two biaxial tests in each family of Table 1: averaged values over the range of increment sizes.

| | family A3 | | | | | | | |
|---|---|---|---|---|---|---|---|---|
| | biaxial test A3-1 | | | | biaxial test A3-2 | | | |
| $\varsigma$ | 1.198 | 1.402 | 1.602 | 1.801 | 1.198 | 1.400 | 1.599 | 1.801 |
| $\arctan(\sigma_{22}/\sigma_{11})$ (deg) | 50.2 | 54.5 | 58.0 | 61.0 | 50.2 | 54.5 | 58.0 | 61.0 |
| $\arctan(\xi_{22}/\xi_{11})$ (deg) | 133.1 | 133.3 | 134.7 | 137.1 | 132.6 | 132.6 | 134.0 | 137.2 |
| $\arctan(\pi_{22}/\pi_{11})$ (deg) | 138.7 | 142.4 | 143.4 | 143.8 | 138.4 | 141.6 | 141.7 | 141.7 |
| | family A4 | | | | | | | |
| | biaxial test A4-1 | | | | biaxial test A4-2 | | | |
| $\varsigma$ | 1.228 | 1.404 | 1.605 | 1.803 | 1.228 | 1.403 | 1.604 | 1.802 |
| $\arctan(\sigma_{22}/\sigma_{11})$ (deg) | 50.8 | 54.5 | 58.1 | 61.0 | 50.8 | 54.5 | 58.1 | 61.0 |
| $\arctan(\xi_{22}/\xi_{11})$ (deg) | 138.6 | 143.8 | 148.9 | 151.7 | 146.8 | 147.9 | 149.5 | 150.1 |
| $\arctan(\pi_{22}/\pi_{11})$ (deg) | 132.2 | 133.6 | 135.6 | 138.3 | 135.6 | 136.8 | 138.3 | 141.8 |
| | family A5 | | | | | | | |
| | biaxial test A5-1 | | | | biaxial test A5-2 | | | |
| $\varsigma$ | 1.799 | 1.914 | 1.919 | 1.929 | 1.782 | 1.905 | 1.929 | 1.929 |
| $\arctan(\sigma_{22}/\sigma_{11})$ (deg) | 60.9 | 62.4 | 62.5 | 62.6 | 60.7 | 62.3 | 62.6 | 62.6 |
| $\arctan(\xi_{22}/\xi_{11})$ (deg) | 153.2 | 154.0 | 154.0 | 155.3 | 153.2 | 154.4 | 152.9 | 153.4 |
| $\arctan(\pi_{22}/\pi_{11})$ (deg) | 138.7 | 142.4 | 143.4 | 143.8 | 138.4 | 141.6 | 141.7 | 141.7 |
| | family B3 | | | | | | | |
| | biaxial test B3-1 | | | | biaxial test B3-2 | | | |
| $\varsigma$ | 1.199 | 1.401 | 1.601 | 1.801 | 1.200 | 1.401 | 1.600 | 1.800 |
| $\arctan(\sigma_{22}/\sigma_{11})$ (deg) | 50.2 | 54.5 | 58.0 | 61.0 | 50.2 | 54.5 | 58.0 | 60.9 |
| $\arctan(\xi_{22}/\xi_{11})$ (deg) | 140.8 | 145.4 | 149.4 | 152.8 | 140.7 | 144.9 | 148.9 | 152.8 |
| $\arctan(\pi_{22}/\pi_{11})$ (deg) | 130.3 | 133.9 | 137.9 | 141.1 | 130.8 | 133.9 | 137.5 | 141.9 |
| | family B4 | | | | | | | |
| | biaxial test B4-1 | | | | biaxial test B4-2 | | | |
| $\varsigma$ | 1.202 | 1.401 | 1.600 | 1.800 | 1.202 | 1.403 | 1.601 | 1.800 |
| $\arctan(\sigma_{22}/\sigma_{11})$ (deg) | 50.2 | 54.5 | 58.0 | 60.9 | 50.2 | 54.5 | 58.0 | 60.9 |
| $\arctan(\xi_{22}/\xi_{11})$ (deg) | 141.5 | 145.8 | 146.2 | — | 140.1 | 146.3 | 149.0 | 152.2 |
| $\arctan(\pi_{22}/\pi_{11})$ (deg) | 130.8 | 135.0 | 136.5 | 141.5 | 131.3 | 136.0 | 139.6 | 140.9 |
| | family B5 | | | | | | | |
| | biaxial test B5-1 | | | | biaxial test B5-2 | | | |
| $\varsigma$ | 1.200 | 1.399 | 1.605 | 1.799 | 1.206 | 1.401 | 1.600 | 1.804 |
| $\arctan(\sigma_{22}/\sigma_{11})$ (deg) | 50.2 | 54.4 | 58.1 | 60.9 | 50.3 | 54.5 | 58.0 | 61.0 |
| $\arctan(\xi_{22}/\xi_{11})$ (deg) | 142.1 | 145.1 | 148.9 | 152.5 | 141.2 | 146.4 | 150.0 | 152.0 |
| $\arctan(\pi_{22}/\pi_{11})$ (deg) | 133.4 | 135.2 | 137.4 | 140.7 | 131.9 | 136.1 | 138.9 | 142.2 |

shear stress component $\sigma_{12}$. This simplifying choice ensures anyway that we have access to the highest values of plastic deformation increments. As was the case for biaxial stress probing, the increments are applied along sixteen equally distributed directions of our stress plane, from 1A to 1P, and vary in amplitude from $\|\delta\boldsymbol{\sigma}\| = 2\sqrt{2}P \times 10^{-3}$ to $\|\delta\boldsymbol{\sigma}\| = 12 \times 2\sqrt{2}P \times 10^{-3}$ (see Fig 8). Points of this plane will be mapped by coordinates computed as $\boldsymbol{\sigma}\cdot\boldsymbol{\xi}/P$ and $\sqrt{2}\sigma_{12}$, where the factor $\sqrt{2}$ is adopted, due to the tensorial nature of $\delta\boldsymbol{\sigma}$, so to visualise families of equal-norm increments as circles.

In order to discuss the validity of the partition hypothesis under rotation of principal stress axes, we refer once more to Eq. 10 as a definition for plastics strain increments. The consequence of this choice is shown in Fig. 9, for a specimen with stress ratio $\varsigma \simeq 1.8$ and loading history from a biaxial test of family A4. Elastic and plastic strain increments are plotted in coordinates of type $\sqrt{2}\,\delta\boldsymbol{\varepsilon}\cdot\boldsymbol{\pi}$ and $\delta\varepsilon_{12}$, i.e., we study exclusively the components of strain increment along a plane parallel to the plastic flow direction $\boldsymbol{\pi}$, found during biaxial stress probing, and orthogonal to the biaxial strain plane. Due to $\boldsymbol{\pi}$ and for reasons of symmetry of the mechanical response, the plastic strain increments are expected to be confined to this plane. Fig. 10 confirms this expectation showing that the plastic response is negligible along a third plane, chosen orthogonal to the biaxial strain plane and to the one in Fig. 9.

The plot in Fig. 9 completes the one in Fig. 5 ($\varsigma \simeq 1.8$) and shows, compared to it, that stress increments inducing

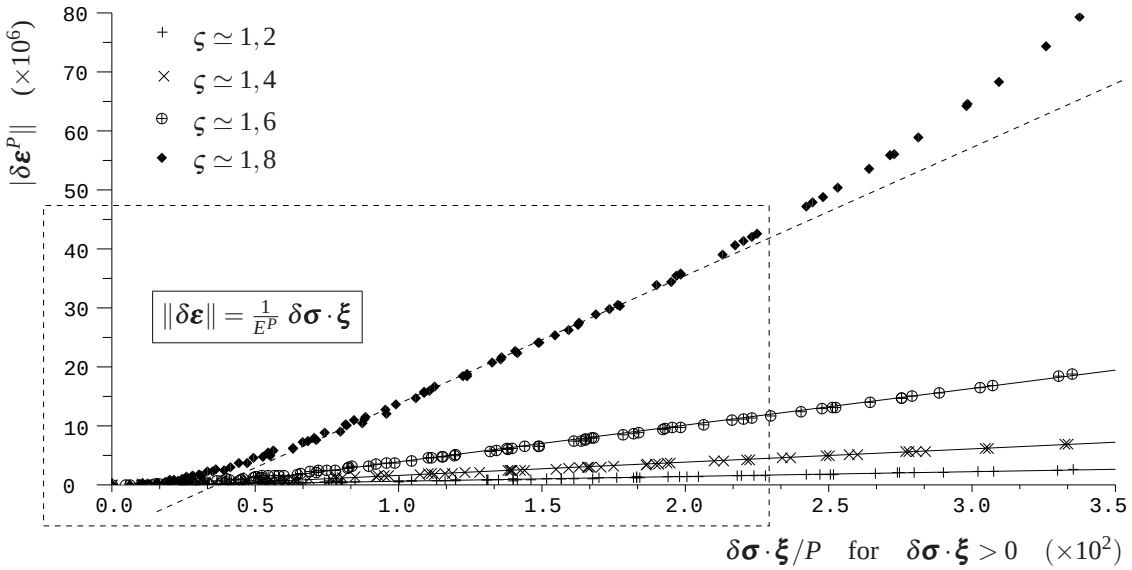


**FIGURE 7.** Plastic strain increment amplitude *vs.* active part of the stress increments for specimens at stress ratios $\varsigma \simeq 1.2$ to 1.8 from a biaxial test of family A4.

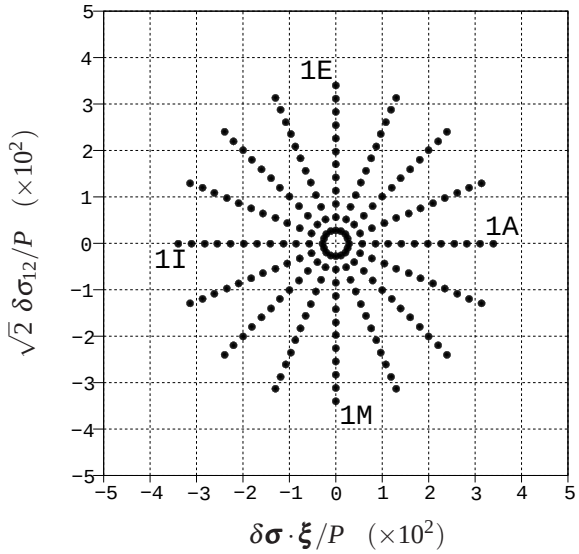


**FIGURE 8.** Rose of applied increments for stress probing with rotation of principal stress axes: 16 increment directions (1A to 1P) for 12 amplitude values in the plane parallel to $\boldsymbol{\xi}$ (biaxial stress probing) and orthogonal to the biaxial stress plane.

rotation of principal stress axes cause, at least, loss of uniqueness of the plastic flow direction. One notices in Fig. 9 as many plastic strain increment directions as the number of stress increment directions: dotted lines in the figure are drawn on naked-eye visible experimental point to show that plastic strain increments originated by proportional stress increments align along precise directions. The question arises whether or not this kind of incremental behaviour is representative of a non-trivial flow rule, or should be modelled in a different constitutive framework than the elastoplastic one. The issue of the flow rule cannot be treated anyway isolated from that of the yield criterion, which is considered next.

A final remark on Fig. 10 is that the envelopes of the plastic response, traced in figure for three different values of the stress increment, obey loosely the symmetry with respect to the axis corresponding to direction $\boldsymbol{\pi}$. It is questionable whether or not the appreciable deviation from symmetry would disappear for REV's of larger sizes.

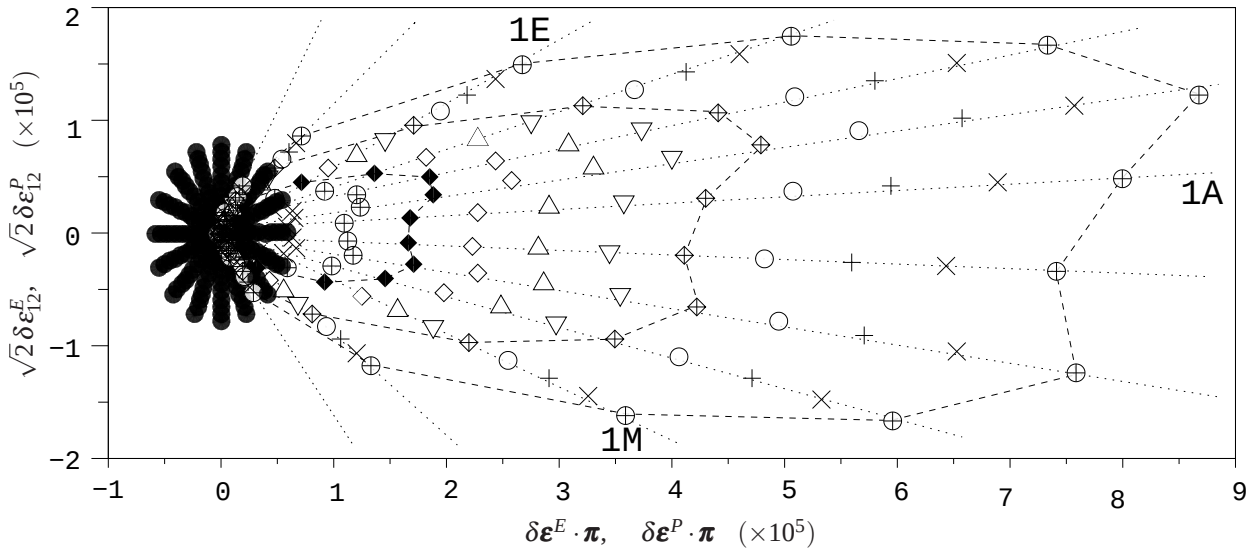


**FIGURE 9.** Elastic strain increments (solid circular marks) and plastic strain increments (other marks, resp.) for a specimen at stress ratio $\varsigma = 1.8$ from a biaxial test of family A4. Dotted lines show the alignment of plastic strain increments for proportional stress increments while dashed segments mark the response envelopes at increments of norm $\|\delta\boldsymbol{\sigma}\| = 4\times 2\sqrt{2}P$, $8\times 2\sqrt{2}P$ and $12\times 2\sqrt{2}P$.

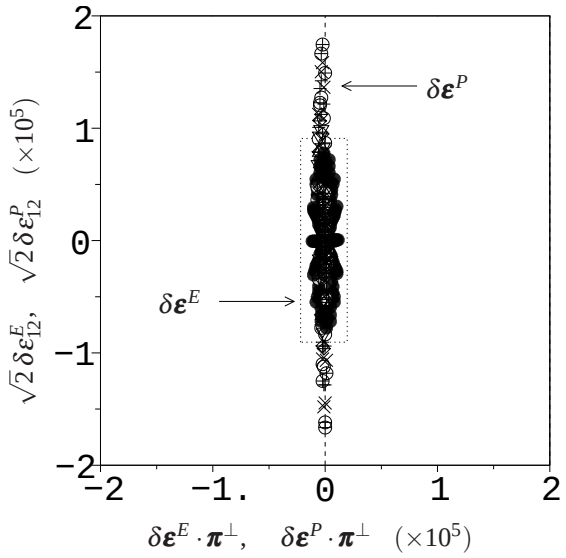


**FIGURE 10.** Elastic strain increments (solid circular marks) and plastic strain increments (other marks, resp.) for a specimen at stress ratio $\varsigma = 1.8$ from a biaxial test of family A4. The representation is given in a strain increment plane orthogonal to those in Fig. 9 and 5: the direction $\boldsymbol{\pi}^\perp$, $\|\boldsymbol{\pi}^\perp\| = 1$, belongs to the biaxial plane and lays orthogonal to $\boldsymbol{\pi}$ ($\arctan(\pi^\perp_{22}/\pi^\perp_{11}) = 138.3^\circ + 90^\circ$, cf. Table 2).

## Yield criterion

The shapes of the envelopes of the elastic and plastic responses are represented in Fig. 11-a for a specimens selected at stress ratio $\varsigma \simeq 1.2$ from a biaxial test of family A5. Due to the low level of stress ratio, the plastic envelope is still bounded by the elastic one and the plastic strain increments related to stress increments of pure shear are dominant with respect to "biaxial" strain increment (parallel to $\boldsymbol{\pi}$). The open shape of the plastic strain envelope denies the existence of a uniquely defined flow rule (cf. Fig 9).

The behaviour shown in fig. 11-a can still be modelled anyway as elastoplastic, provided one drops the assumption of a unique mechanism of plastic deformation [26, 27]. We postpone a detailed exposition of our idea to a further publication and give here an example of the procedure to fit the case in the figure with a first generalisation of the classical elastoplastic framework. We consider in particular the possibility of three distinct and independent plastic mechanisms of deformation: a first mechanism detectable with biaxial stress probes and two pseudo-symmetric additional mechanisms activated by shear stress increments of positive and negative values, respectively. The partition hypothesis now writes in the form

$$\delta\boldsymbol{\varepsilon} = \delta\boldsymbol{\varepsilon}^E + \delta\boldsymbol{\varepsilon}^P_I + \delta\boldsymbol{\varepsilon}^P_{II} + \delta\boldsymbol{\varepsilon}^P_{III} \tag{11}$$

where the amplitudes of the three separate plastic increments on the r.h.s. are given by the respective yield criteria, i.e.,

$$\|\delta\boldsymbol{\varepsilon}^P_I\| = \begin{cases} \frac{1}{E^P_I}\,\delta\boldsymbol{\sigma}\cdot\boldsymbol{\xi}_I & \text{if} \quad f(\boldsymbol{\sigma})=0 \quad \text{and} \quad \delta\boldsymbol{\sigma}\cdot\boldsymbol{\xi}_I \geq 0 \\ 0 & \text{if} \quad f(\boldsymbol{\sigma})=0 \quad \text{and} \quad \delta\boldsymbol{\sigma}\cdot\boldsymbol{\xi}_I < 0 \\ 0 & \text{if} \quad f(\boldsymbol{\sigma})<0 \end{cases}, \tag{12}$$

$$\|\delta\boldsymbol{\varepsilon}^P_{II}\| = \begin{cases} \frac{1}{E^P_{II}}\,\delta\boldsymbol{\sigma}\cdot\boldsymbol{\xi}_{II} & \text{if} \quad f(\boldsymbol{\sigma})=0 \quad \text{and} \quad \delta\boldsymbol{\sigma}\cdot\boldsymbol{\xi}_{II} \geq 0 \\ 0 & \text{if} \quad f(\boldsymbol{\sigma})=0 \quad \text{and} \quad \delta\boldsymbol{\sigma}\cdot\boldsymbol{\xi}_{II} < 0 \\ 0 & \text{if} \quad f(\boldsymbol{\sigma})<0 \end{cases}, \tag{13}$$

$$\|\delta\boldsymbol{\varepsilon}^P_{III}\| = \begin{cases} \frac{1}{E^P_{III}}\,\delta\boldsymbol{\sigma}\cdot\boldsymbol{\xi}_{III} & \text{if} \quad f(\boldsymbol{\sigma})=0 \quad \text{and} \quad \delta\boldsymbol{\sigma}\cdot\boldsymbol{\xi}_{III} \geq 0 \\ 0 & \text{if} \quad f(\boldsymbol{\sigma})=0 \quad \text{and} \quad \delta\boldsymbol{\sigma}\cdot\boldsymbol{\xi}_{III} < 0 \\ 0 & \text{if} \quad f(\boldsymbol{\sigma})<0 \end{cases}, \tag{14}$$

and by the respective flow rules, grouped here below:

$$\forall\delta\boldsymbol{\sigma}: \begin{cases} \delta\boldsymbol{\varepsilon}^P_I(\delta\boldsymbol{\sigma}) = \boldsymbol{\pi}_I(\boldsymbol{\sigma})\,\|\delta\boldsymbol{\varepsilon}^P_I(\delta\boldsymbol{\sigma})\| \\ \delta\boldsymbol{\varepsilon}^P_{II}(\delta\boldsymbol{\sigma}) = \boldsymbol{\pi}_{III}(\boldsymbol{\sigma})\,\|\delta\boldsymbol{\varepsilon}^P_{II}(\delta\boldsymbol{\sigma})\| \\ \delta\boldsymbol{\varepsilon}^P_{III}(\delta\boldsymbol{\sigma}) = \boldsymbol{\pi}_{II}(\boldsymbol{\sigma})\,\|\delta\boldsymbol{\varepsilon}^P_{III}(\delta\boldsymbol{\sigma})\| \end{cases} \tag{15}$$

We identify in particular $\boldsymbol{\xi}_I$ to the normal to the criterion detected by the biaxial stress probing procedure, i.e. $\boldsymbol{\xi}_I \equiv \boldsymbol{\xi}$, and seek $\boldsymbol{\xi}_{II}$ and $\boldsymbol{\xi}_{III}$ in the plane of Fig. 8. Analogously we set $\boldsymbol{\pi} \equiv \boldsymbol{\pi}_I$ and pick $\boldsymbol{\pi}_{II}$ and $\boldsymbol{\pi}_{III}$ in the plane of Fig. 11-a.

As to the fitting of the flow rule, compared to the case in Fig. 6, one is now bound to use the sum of three truncated cosine functions, one for each of the three orthogonal criteria in Eqs. 12-14:

$$\delta\boldsymbol{\varepsilon} = \left( \frac{[\cos(\theta-\theta_I)]^+}{E^P_I}\boldsymbol{\pi}_I + \frac{[\cos(\theta-\theta_{II})]^+}{E^P_{II}}\boldsymbol{\pi}_{II} + \frac{[\cos(\theta-\theta_{III})]^+}{E^P_{III}}\boldsymbol{\pi}_{III} \right) \|\delta\boldsymbol{\sigma}\| \tag{16}$$

where $[\cdot]^+$ denotes the positive part of the argument function and the angles $\theta$, $\theta_I$, $\theta_{II}$ and $\theta_{III}$, are measured counterclockwise in the plane of Fig. 8 starting from direction $\boldsymbol{\xi}$. Angles $\theta_I$, $\theta_{II}$ and $\theta_{III}$, refer to $\boldsymbol{\xi}_I$, $\boldsymbol{\xi}_{II}$ and $\boldsymbol{\xi}_{III}$, respectively (e.g. $\theta_I = 0$). Our fitting parameters are the angles $\theta_{II}$ and $\theta_{III}$, the three plastic moduli $E^P_I$, $E^P_{II}$, $E^P_{III}$ and the angles $\omega_{II}$ and $\omega_{III}$ referred to $\boldsymbol{\pi}_{II}$ and $\boldsymbol{\pi}_{III}$ and measured counterclockwise in the plane of Fig. 11 starting from $\boldsymbol{\pi}$ (e.g. $\omega_I = 0$). The quality of the fitting in Fig. 12 is encouraging. We remark anyway that this setting does not apply immediately to the cases with highest stress ratio (i.e., $\varsigma \simeq 1.6$ and $\varsigma \simeq 1.8$) where some degree further generality needs to be added to the model.

To conclude on the case in Fig. 11a and validate our renewed partition hypothesis, we plot in Fig. 11b the difference $\delta\boldsymbol{\varepsilon}^P - \delta\boldsymbol{\sigma}\cdot\boldsymbol{\xi}_I/E^P_I$ in order to visualise the response envelope exclusively for the plastic increments of competence of the second and third mechanisms, i.e., $\delta\boldsymbol{\varepsilon}^P_{II}$ and $\delta\boldsymbol{\varepsilon}^P_{III}$. The plastic envelop in the figure now conforms to two clearly-defined directions, i.e. the two "missing" flow directions $\boldsymbol{\pi}_{II}$ and $\boldsymbol{\pi}_{III}$.

## CONCLUSION

Our concern in this work is an assessment of some features of the elastoplastic behaviour of granular materials and an evaluation on the representativity of the measurements that can be obtained from the stress probing procedure

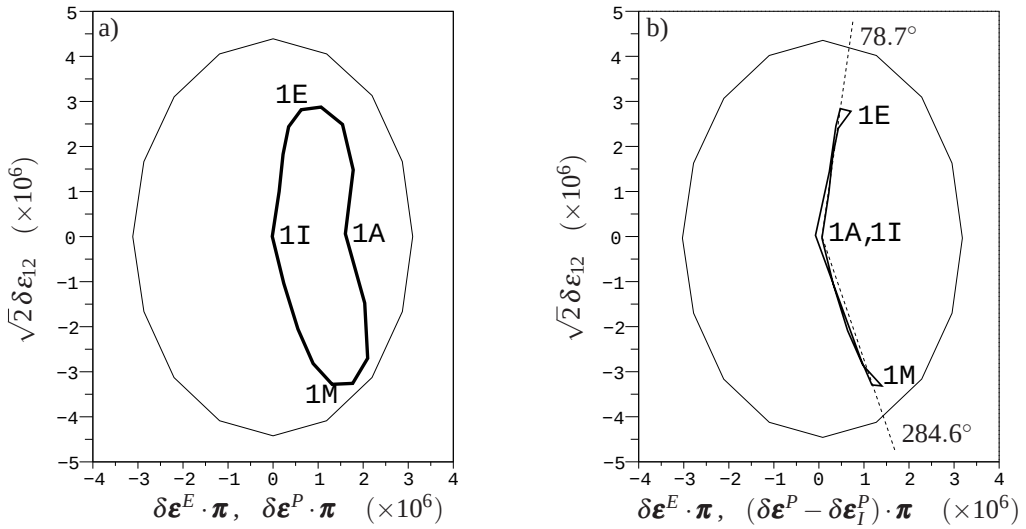


**FIGURE 11.** Elastic and plastic response envelopes for specimen at stress ratio $\varsigma \simeq= 1.2$, from a biaxial test of family A4, under stress increments of amplitude $2\times 2\sqrt{2}P$ in Fig. 8. Total plastic response $\delta\boldsymbol{\varepsilon}^P$ (a) or plastic response for mechanisms II and III (b). .

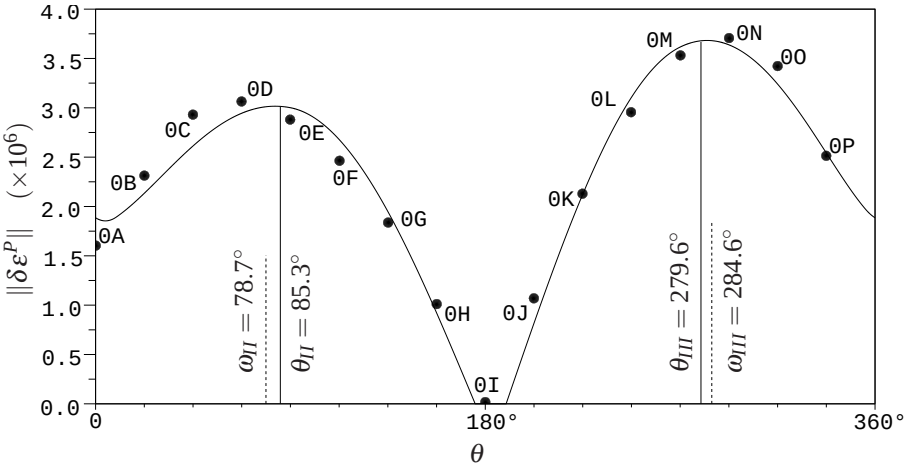


**FIGURE 12.** Fitting of the plastic strain increment amplitude with Eq. 16, for specimen at stress ratio $\varsigma = 1.2$, from a biaxial test of family A4, under stress increments of amplitude $2\times 2\sqrt{2}P$ in Fig. 8.

*via* DEM simulations. To this extent, our study was conceived in parametrical form, and we play on the size of the stress increments, the stiffness parameter $\kappa = K_N/P$ and the stress ratio $\varsigma$, within two distinct qualitative classes of deformation response (cf. Table 1 and Fig. 1-2). The results presented here were obtained from a limited number of prototype stress probing tests.

For the case of stress probes in the biaxial stress plane we observed the existence of a clear direction of accumulation for plastic strain increments, i.e. a plastic flow direction in the language of plasticity. Measurements of this quantity were robust, i.e. not affected significantly by the stress increment size. On the other hand both the normal to the yield criterion and the plastic modulus $E^P$ were found sensitive to the increment size, especially the latter. We propose in particular that a criterion for the detection of the appropriate range of stress increments should be based on a requirement of linearity between plastic strain increments and "active" stress increments (cf. Fig. 7) with stable coefficient $1/E^P$.

The normal to the yield criterion was found systematically orthogonal, with very good approximation, to the load direction. According to the presentation in the introduction and to Eq. 9, this is the explicit signature of a yield criterion

of the Mohr-Coulomb type in the sense of the pastic slip theory. All in all the response of the tested specimens to stress probes in the biaxial stress plane can be certainly ascribed to the class of elastoplastic materials with single mechanism of plastic deformation, as found in the literature [10, 11, 12]. A variable difference in angle, of the order of $10^\circ$, was observed between the plastic flow direction and the normal to the yield criterion, confirming the non associated character of the flow rule.

As to the incremental response to stress probes with rotation of principal stress axes, i.e. with non-null tangential components, the first remark concerns the loss of a uniquely defined plastic flow direction. The stress increment were applied in a plane orthogonal to the biaxial plane and parallel to the (biaxial) normal to the yield criterion. The plastic strain increments were found exclusively in the plane orthogonal to the biaxial plane and parallel to the (biaxial) plastic flow direction. We showed that this scenario can still be modelled in the elastoplastic framework by introducing additional mechanisms of plastic deformation.

The above features were observed for the different values of parameters and classes of qualitative behaviour, but a study of their quantitative variability is part of the work to come.

## ACKNOWLEDGMENTS

Laboratoire Navier is a joint research unit of Laboratoire Central des Ponts et Chaussées, Ecole Nationale des Ponts et Chaussées and Centre National de la Recherche Scientifique. PPF CEGEO is a joint programme funded by the French Ministry of Higher Education and Research.

## REFERENCES

1. J. K. Mitchell, *Fundamentals of soil behavior*, Wiley, New York, 1993.
2. P. A. Vermeer, in *Physics of Dry Granular Media*, edited by H. J. Herrmann, J.-P. Hovi, and S. Luding, Balkema, Dordrecht, 1998, pp. 163–96.
3. F. Alonso-Marroquín, S. Luding, H. J. Herrmann, and I. Vardoulakis, *Phys. Rev. E* **71**, 051304 (2005).
4. C. Tamagnini, F. Calvetti, and G. Viggiani, *J. Eng. Math.* **52**, 265–91 (2005).
5. F. Darve, L. Sibille, A. Daouadji, and F. Nicot, *C. R. Mécanique* **335**, 496–515 (2007).
6. F. Radjaï, *eprint ArXiv:0801.4722v1* (2008).
7. P. Royis, and T. Doanh, *Int. Journ. Num. Anal. Methods in Geomechanics*, **22**, 34-45, (1998).
8. J. P. Bardet, and J. Proubet, in *Powders and Grains 1989*, edited by J. Biarez, and R. Gourvès, Balkema, Rotterdam, 1998, pp. 265–73.
9. J. P. Bardet, *Int. J. of Plasticity*, **10**, 879–908 (1994).
10. F. Calvetti, G. Viggiani and C. Tamagnini, *Constitutive modelling and analysis of boundary value problems in geotechnical engineering*, edited by G. Viggiani, Hevelius, Benevento, 187–216 (2003).
11. F. Calvetti, G. Viggiani and C. Tamagnini, *Rivista italiana di geotecnica*, **3**, 11–29 (2003).
12. F. Alonso-Marroquín, and H. J. Herrmann, *Phys. Rev. E* **66**, 021301 (2002).
13. J.-N. Roux, and G. Combe, *Comptes-Rendus Physique*, **3**, 131–40 (2003).
14. I. Agnolin, and J.-N. Roux, *Phys. Rev. E* **76**, 061304 (2007).
15. I. Agnolin, and J.-N. Roux, *Phys. Rev. E* **76**, 061302 (2007).
16. J.-N. Roux, and G. Combe, these proceedings.
17. W. Prager, and D. C. Drucker, *Q. Appl. Mathematics*, **2**, 157–65 (1952).
18. K. H. Roscoe, A. N. Schofield, and C. P. Wroth, *Geotechnique*, **8**, 22–53 (1958).
19. A. N. Schohield, and C. P. Wroth, *Critical State Soil Mechanics*, McGraw-Hill (1968).
20. S. B. Batdorf, and B. Budiansky, NACA TN 1871 (1949).
21. J. Desrues, and R. Chambon, *Int. J. Solid Struct.* **39**, 3757–76 (2002).
22. J. W. Rudnicki, and J. R. Rice, *J. Mech. Phys. Solids* **23**, 371–94 (1975).
23. M. Allen, and D. Tildesley, *Computer simulations of liquids*, Oxford University Press, Oxford, 1987.
24. P.-E. Peyneau, and J.-N. Roux, *Phys. Rev. E* **78**, 011307 (2008).
25. J.-N. Roux, in *Powders and Grains 2005*, edited by R. García Rojo, H. J. Herrmann, and S. McNamara, Balkema, Leiden, 2005, pp. 261–5.
26. W. T. Koiter, *Quart. Appl. Math.*, **2**, 350–4 (1953).
27. R. Baldacci, G. Ceradini, and E. Giangreco, *Plasticità*. CISIA, Milan, 1974, pp. 11–56.